Ca²⁺-induced Recruitment of the Secretory Vesicle Protein DOC2B to the Target Membrane*⒮

Alexander J. A. Groffen‡, Elisabeth C. Brian, Jeroen J. Dudok, Joris Kampmeijer, Ruud F. Toonen, and Matthijs Verhage

From the Department of Functional Genomics, Center for Neurogenomics and Cognition Research, Vrije Universiteit, De Boelelaan 1085, Amsterdam 1081 HV, The Netherlands

Ca²⁺-dependent fusion of transport vesicles at their target can be enhanced by intracellular Ca²⁺ and diacylglycerol. Diacylglycerol induces translocation of the vesicle priming factor Munc13 and association of the secretory vesicle protein DOC2B to the membrane. Here we demonstrate that a rise in intracellular Ca²⁺ is sufficient for a Munc13-independent recruitment of DOC2B to the target membrane. This novel mechanism occurred readily in the absence of Munc13 and was not influenced by DOC2B mutations that abolish Munc13 binding. Purified DOC2B (expressed as a bacterial fusion protein) bound phospholipids in a Ca²⁺-dependent way, suggesting that the translocation is the result of a C2 domain activation mechanism. Ca²⁺-induced translocation was also observed in cultured neurons expressing DOC2B-enhanced green fluorescent protein. In this case, however, various degrees of membrane association occurred under resting conditions, suggesting that physiological Ca²⁺ concentrations modulate DOC2B localization. Depolarization of the neurons induced a complete translocation of DOC2B-enhanced green fluorescent protein to the target membrane within 5 s. We hypothesize that this novel Ca²⁺-induced activity of DOC2B functions synergistically with diacylglycerol-induced Munc13 binding to enhance exocytosis during episodes of high secretory activity.

Ca²⁺-induced exocytosis is a widely conserved mechanism of importance for a broad range of secretory systems, such as the release of neurotransmitters and neuropeptides in the central and peripheral nervous system. To attain fusion competence, secretory vesicles must first dock at the target membrane and undergo a process called priming. The release of fusion-ready vesicles is coupled to the opening of Ca²⁺ channels in the plasma membrane, producing a transient high Ca²⁺ concentration (10–100 μM for ~1 ms) in close proximity to the channels. The inward Ca²⁺ current then diffuses into the cytoplasm, resulting in a residual concentration in the range of 1 μM during tens of seconds. It is widely accepted that this residual Ca²⁺ concentration induces short term changes in exocytotic strength (*e.g.* see Refs. 1 and 2), although the mechanisms that

contribute to this phenomenon remain largely unclear. As a result, the secretory strength of neuronal and endocrine release sites is modulated in an activity-dependent way. This phenomenon is important to avoid vesicle depletion during repetitive stimulation and is furthermore considered in neurons to contribute to memory and learning.

Although Ca²⁺ is the most important messenger after high frequency activation of the release site, exocytotic potentiation can also be induced by diacylglycerol (synthesized by members of the phospholipase family) or by its phorbolester analogues. Diacylglycerol has multiple intracellular targets (*e.g.* protein kinase C isoforms), but the potentiating effect in regulated exocytosis is mediated by the priming factor Munc13-1. Munc13-1-deficient mice die shortly after birth and show a defect in synaptic vesicle exocytosis from glutamatergic synapses, presumably due to an arrest between the docking and fusion steps of the synaptic vesicle cycle (3). In another study, the Munc13-1 gene was replaced with the allele Munc13-1^H567K, encoding a mutant protein that specifically lacks diacylglycerol-binding activity. Hippocampal neurons from homozygous Munc13-1^H567K mice show normal evoked postsynaptic currents (4). However, the readily releasable pool size is diminished, the recovery from high frequency stimulation is slowed down, and the potentiating effect of phorbolesters is blocked (4). Thus, Munc13-1 may enhance vesicle priming during high frequency stimulation through acting as a diacylglycerol sensor. Several studies have suggested that the potentiating activity of Munc13 involves its interaction with proteins of the DOC2 family, as discussed below.

The DOC2 protein family comprises three isoforms, designated DOC2A, -B, and -C. The latter is predominantly expressed in the heart (5). DOC2A and DOC2B are both expressed in the brain, and in addition DOC2B is found in several peripheral tissues (6, 7). In subcellular fractionations, DOC2A and -B copurify with secretory vesicles, although they lack a transmembrane domain. DOC2 proteins consist of three structural domains: a short N-terminal domain and two C2 domains named C2A and C2B, respectively, similar to those in synaptotagmins and protein kinase C (PKC).[1] This presence of these motifs predicts a Ca²⁺-binding function. For DOC2B, this was experimentally confirmed *in vitro*; Ca²⁺ induced binding of the isolated C2A domain to phosphatidylserine-containing liposomes with half-maximal binding at 1 μM Ca²⁺ (8). A positive function in secretion was suggested by the increased release of growth hormone from PC12 cells overexpressing DOC2A (9).

Both DOC2A and -B bind Munc13-1 in a diacylglycerol-de-

⒮ The on-line version of this article (available at http://www.jbc.org) contains three movies.

‡ To whom correspondence should be addressed. Tel.: 31-20-4446928; Fax: 31-20-4446926; E-mail: sander@cncr.vu.nl.

[1] The abbreviations used are: PKC, protein kinase C; EGFP, enhanced green fluorescent protein; GST, glutathione *S*-transferase; TIRF, total internal reflection fluorescence; PBS, phosphate-buffered saline; MAP2, microtubule-associated protein 2.

TABLE I
*Names of mutant DOC2B molecules generated by
site-directed mutagenesis*

For each mutant, the introduced mutation and its effect on DOC2B function are described. Numbers indicate amino acids. For both mutants, the described effect is proven experimentally (12, 20).

Name	Mutation	Effect
TCT	Δ2–9	Blocks Tctex-1 binding
M13	Substitution of amino acids 15–20 (QEHMAI to YKDWAF)	Blocks Munc13 binding

pendent manner (10). This interaction is mediated by the Munc13-interacting domain located within the N-terminal domain of DOC2. Interestingly, diacylglycerol also induces a Munc13-1-dependent translocation of DOC2B to the plasma membrane in HEK293 cells (11). Injection of a synthetic peptide identical to the Munc13-interacting domain region into cholinergic neurons of the superior cervical ganglion was shown to inhibit synaptic transmission in an activity-dependent manner (12). Similarly, injection of this peptide into the Calyx of Held blocked the potentiating effect of phorbolester administered 5 min after the peptide (13). Together, these data suggest that the DOC2-Munc13 interaction contributes to the mechanism of diacylglycerol-induced presynaptic potentiation.

DOC2 proteins also bind to Munc18, a syntaxin-binding protein that is required for neurotransmitter secretion (7, 14). In chromaffin cells of the adrenal gland, homozygous Munc18 null mice showed a 10-fold reduction in morphologically docked vesicles and a corresponding reduction in Ca^{2+}-dependent exocytosis of large dense core vesicles (15). Many overexpression studies with Munc18 homologs have been reported with seemingly conflicting results, in general supporting the hypothesis that Munc18 exerts its function in the final stages upstream from Ca^{2+}-induced vesicle exocytosis at least in mammalian systems (16).

Here we describe a novel mechanism for the translocation of DOC2B to the membrane, triggered by intracellular Ca^{2+}. In contrast to the diacylglycerol-induced translocation, Ca^{2+}-dependent translocation occurs independent of Munc13 binding. Since diacylglycerol and Ca^{2+} activation generally coincide during episodes of high secretory activity, we hypothesize that both mechanisms may act in concert to increase the exocytotic strength.

EXPERIMENTAL PROCEDURES

Antibodies—A polyclonal antibody designated 13.2 was raised against DOC2B by immunizing New Zealand White rabbits with 500 μg of a bacterially expressed polypeptide comprising amino acids 22–116 of DOC2B. The serum recognized a single protein of the expected molecular mass as determined by Western blotting using rat brain homogenate. It also reacted strongly with lysate from HEK293 cells expressing fusion proteins consisting of DOC2B and enhanced green fluorescent protein (EGFP) but not EGFP alone. The mouse monoclonal anti-Myc tag antibody 9E10 and the mouse monoclonal anti-EGFP antibody B34 were purchased from Babco (Richmond, CA).

Construction of Expression Vectors—A cDNA fragment encoding full-length wild type DOC2B (GenBank™ accession number U70778) was amplified by polymerase chain reaction with the DNA polymerase PfuI (Stratagene, La Jolla, CA) using the rat cDNA clone pNP3a as template (7). The sense primer (5′-ttggtacccgctgacttacccccc-3′) introduces a KpnI restriction site 69 nucleotides upstream of the start codon; the antisense primer (5′-gcggatcccgtcgtcgagtacagc-3′) removes the stop codon and introduces a BamHI restriction site. This fragment was introduced into pEGFP-N2 (Clontech) using the corresponding sites. Expression vectors encoding Myc-tagged DOC2B were derived from this vector by subcloning the NheI-BamHI fragment into the corresponding sites of pCDNA3.1-Myc-HisC (Invitrogen). Expression vectors encoding Munc13-1, PKC-α, and PKC-γ were described previously (17–19).

Site-directed Mutagenesis—Complementary DNAs encoding the mutant fusion proteins listed in Table I were generated by site-directed

mutagenesis, performed by full-length amplification of the pEGFP-N2-DOC2B expression vector with mutagenic primers. PfuI DNA polymerase (Roche Applied Science) was used for amplification. Template DNA was selectively degraded by incubation with DpnI endonuclease, and the PCR product was introduced into *Escherichia coli* DH5α. The integrity of all mutant cDNAs was confirmed by sequence analysis of the complete open reading frame on a Beckman CEQ 2000 automated sequencer (Fullerton, CA). All DOC2B variants (wild type and mutant) were also subcloned into pCDNA3.1 and pCDNA3.1-Myc (Invitrogen).

Cell Culture—HEK293 (ATCC CRL 1573) were cultured at 37 °C in the presence of 5% (v/v) CO$_2$ in Dulbecco's modified Eagle's medium containing sodium pyruvate, pyridoxine, and 1 g/liter glucose (Invitrogen) supplemented with 10% heat-inactivated fetal calf serum (Invitrogen), 1 mM glutamine, 1× nonessential amino acids (Gibco), 200 IU/ml penicillin, and 200 μg/ml streptomycin. One day after seeding on glass coverslips in 6-well plates, the cells were transfected with 2.5 μg of vector DNA using the standard calcium phosphate precipitation method. For co-expression of Munc13-1, the expression vector pCDNA3-Munc13-1 was added in a 3-fold molar excess over pEGFP-DOC2B. Medium was refreshed at 16 and 40 h, and translocation assays were performed at 48–50 h post-transfection. PC12 cells were cultured on 18-mm glass coverslips in Dulbecco's modified Eagle's medium containing 10% horse serum, 5% fetal calf serum, 4 mM L-glutamine, 100 IU/ml penicillin, and 100 μg/ml streptomycin in the presence of 5% CO$_2$. Cells were transfected with 2 μg of vector DNA using LipofectAMINE 2000 (Invitrogen), and measurements (by total internal reflection fluorescence microscopy) were conducted 6–8 h post-transfection. Neurons were isolated from C57BL/6 mouse embryos at day 18 of gestation and seeded at 25,000 cells/cm^2 in 12-well plates on poly-L-lysine-coated coverslips in neurobasal medium (Invitrogen) supplemented with B-27 supplement (Invitrogen). The cells were cultured at 37 °C in a humidified chamber gassed with 5% CO$_2$. Six h after seeding, the neurons were transduced with lentiviral particles using a multiplicity of infection of 1.5–2 infective particles/cell.

Western Blotting—Fourty-eight h post-transfection, HEK293 cells were lysed in 10 mM Tris-HCl, pH 7.4, 1 mM EDTA, and 1% Triton X-100. The lysate was cleared by centrifugation for 30 min at 16,000 × g, followed by electrophoresis on a 6–15% Tris-glycine gradient gel. Proteins were transferred to a polyvinylidine difluoride membrane (Bio-Rad). Membranes were incubated for 16 h at 4 °C in 5% blocking agent (Amersham Biosciences) dissolved in TBST (20 mM Tris, 137 mM NaCl, and 0.1% Tween 20), washed, and incubated with anti-GFP (Covance Research Products, Denver, PA; diluted 1:25,000) or anti-Doc2B (13.2; diluted 1:1,000) for 90 min in TBST. The membranes where washed again and incubated for 1 h with alkaline phosphatase-conjugated goat anti-mouse or goat anti-rabbit secondary antibody (Amersham Biosciences) diluted 1:5,000 in TBST. Finally, the membranes were washed, incubated for 5 min in enhanced chemifluorescence substrate (Amersham Biosciences), and analyzed on a FLA5000 fluoroimager (Raytest, Tilburg, The Netherlands). All incubations were carried out at room temperature unless otherwise stated.

Immunofluorescence Microscopy—Cells were fixed 48 h post-transfection for 15 min in 2% paraformaldehyde (Merck) in PBS and 15 min in 4% paraformaldehyde. Subsequently, they were incubated in PBS containing 4% fetal calf serum (Invitrogen) for 20 min. Next, the cells were incubated with anti-Doc2B antibody 13.2, diluted 1:4,000 in PBS containing 0.1% Triton X-100. As the secondary antibody we used Alexa546-conjugated goat anti rabbit (Molecular Probes, Inc.) diluted 1:1,000 in PBS containing 0.1% Triton X-100. The cells were mounted in Dabco-Mowiol (Sigma) and analyzed on an LSM 510 confocal microscope (Carl Zeiss BV, Weesp, The Netherlands).

Confocal Imaging of Live and Fixed Cells—For imaging of EGFP fluorescence in fixed cells, the cells were incubated for 10 min at 37 °C in basal buffer (25 mM HEPES, pH 7.4, 140 mM NaCl, 4.7 mM KCl, 1.4 mM MgCl$_2$, and 10 mM glucose), in ionophore-containing medium (basal buffer supplemented with 3 mM CaCl$_2$ and 1 μM A23187) or in a depolarizing medium containing 25 mM HEPES, pH 7.4, 90 mM NaCl, 60 mM KCl, 3 mM CaCl$_2$, 1.4 mM MgCl$_2$, and 10 mM glucose. A23187 was purchased from Sigma. In case cells were fixed, this was achieved by adding an equal volume of 4% (w/v) paraformaldehyde to the medium and incubating for 20 min at room temperature. Neurons were then counterstained for microtubule-associated protein 2 (MAP2; a neuron-specific protein located in dendrites) as follows. After fixation, the cells were washed twice with PBS and then incubated for 1 h with a monoclonal antibody recognizing MAP2 (Chemicon; diluted 1:200 in PBS with 0.1% Triton X-100), washed again twice, and incubated in the presence of Alexa546-conjugated goat anti-mouse antibodies (Molecular Probes; diluted 1:000). Confocal imaging was performed with an LSM

510 confocal microscope and a ×63 Plan-Neofluar lens (Carl Zeiss). Fluorescence intensity in regions of interest was quantitated using Multianalyst image analysis software (Bio-Rad). To test statistically if the fluorescence intensity after stimulation was significantly different from that before stimulation, the fluorescence after stimulation was calculated as a percentage of the original value. This was done for each cellular compartment in nine different cells. A two-tailed Student's t test was used to test whether the resulting mean values differed significantly from 100% ($p < 0.005$).

Total Internal Reflection Fluorescence Microscopy—Transfected PC12 cells were incubated in basal solution containing 10 mM HEPES, pH 7.35, 147 mM NaCl, 2.8 mM KCl, 5 mM CaCl₂, 1 mM MgCl₂, and 10 mM glucose. Depolarizing solution (identical except for NaCl (90 mM) and KCl (60 mM)) was applied using a motor-driven two barrel Piezo perfusion device (Warner Instruments, Hamden, CT), allowing for fast (<10-ms) switching between depolarizing and basal solution. Total internal reflection fluorescence (TIRF) microscopy was performed on a Zeiss inverted microscope with custom built TIRF set up (Till Photonics, Grafelfing, Germany), using a ×100 objective with 1.45 numerical aperture. The depth of the evanescent field was measured to be 128 nm. Images were collected at 30 Hz using an intensified CCD camera (I-Pentamax; Roper Scientific) and analyzed with Metamorph (Universal Imaging Corp., Downingtown, PA). Fluorescence intensity was measured in a region of interest over the cell and corrected for background measured outside of the cell.

Expression and Purification of GST-DOC2B—Full-length rat DOC2B cDNA was cloned into the expression vector pGEX4T3 (Amersham Biosciences) to encode a fusion protein of glutathione *S*-transferase (GST) and DOC2B. To isolate GST-DOC2B, 5 liters of Luria broth medium with 100 μg/ml ampicillin and 0.2% glucose was incubated at 37 °C until the exponential growth phase was reached. The incubation was then prolonged for 4 h in the presence of 100 μM isopropyl-1-thio-β-D-galactopyranoside to induce expression. Bacteria were centrifuged for 15 min at 4,000 × *g* and resuspended in 100 ml of HBS buffer (140 mM NaCl, 50 mM HEPES, pH 7.4, and protease inhibitor mixture; Roche Applied Science catalog no. 1836170). The cells were lysed by sonication and incubated for 1 h at 4 °C in the presence of 2.5% Triton X-100 for solubilization. After clearing the lysate by centrifugation for 30 min at 15,000 × *g* and 4 °C, GST-DOC2B was affinity-purified using glutathione-conjugated Sepharose 4B beads (Sigma). The amount of bound protein was determined by eluting GST-DOC2B in HBS plus 10 mM glutathione from a sample of the beads, followed by a Bradford assay using bovine serum albumin as a standard. The final yield of recombinant protein was 1.2 mg/liter of culture volume.

Liposome Binding Assay—³H-Labeled liposomes were prepared by drying a mixture of 125 μl of phosphatidylcholine, 50 μl of phosphatidylserine (both 10 mg/ml in chloroform; Sigma), and 20 μl of 1,2-dipalmitoyl, L-3-phosphatidyl [*N-methyl*-³H]choline (1 mCi/ml; specific activity 83 Ci/mmol; Amersham Biosciences) under a nitrogen gas flow. The phospholipids were suspended in 10 ml of 10 mM HEPES, pH 7.2, and 100 mM NaCl, sonicated for 30 s, and centrifuged for 10 min at 3,000 × *g* to remove aggregates from the liposome suspension. Buffered Ca²⁺ solutions were prepared in 50 mM HEPES, pH 7.20, 140 mM NaCl, and 10 mM EGTA (<1 μM free Ca²⁺) or HEDTA (>1 μM free Ca²⁺) as a chelator. The concentrations of total Ca²⁺ were calculated with Win-Maxc version 2.40 (Chris Patton, Stanford, CA; available on the World Wide Web at www.standford.edu/~cpatton). Liposome binding was assayed in each buffer by incubating 50 μl of a 25% Sepharose slurry containing 50 μg of immobilized GST-DOC2B with 100 μl of the ³H-labeled liposome suspension for 1 h at 20 °C in a total volume of 1.5 ml. The beads were collected by centrifugation for 5 min at 1,000 × *g* and washed with 1.5 ml of the same buffered Ca²⁺ solution. After five washes, bound ³H-labeled phospholipids were eluted from the beads in 0.5% SDS, and radioactivity was quantitated by liquid scintillation counting in UltimaGold mixture (Packard).

RESULTS

To investigate the possibility that DOC2B may function as a Ca²⁺ sensor in the activity-dependent enhancement of exocytosis, we first used heterologous cell lines to analyze whether Ca²⁺ influences the cellular distribution of DOC2B. To focus exclusively on Ca²⁺-dependent mechanisms, we selected HEK293 cells that lack endogenous expression of Munc13, thus excluding the diacylglycerol-induced DOC2B translocation for which Munc13 is required (11). Fusion proteins consisting of full-length DOC2B and EGFP were expressed in HEK293 cells
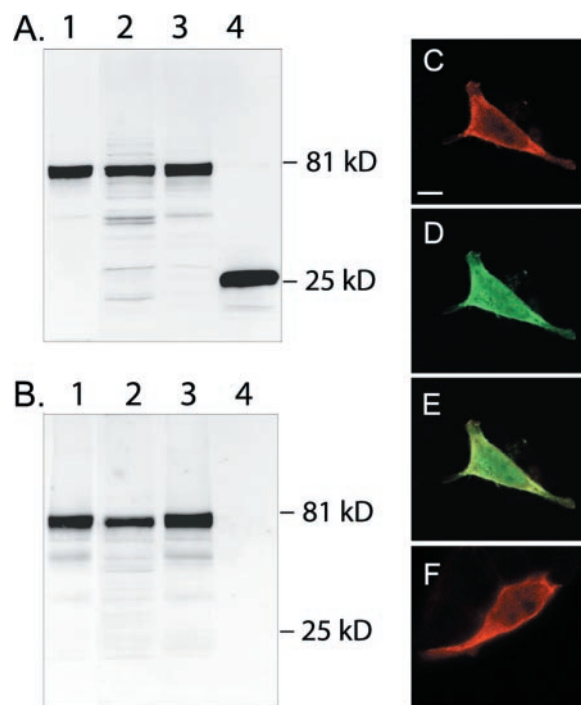

FIG. 1. *A* and *B*, DOC2B-EGFP is expressed in HEK293 cells as a stable fusion protein of the expected molecular mass. HEK293 cells were transfected with expression vectors encoding DOC2B-EGFP fusions (*lanes 1–3*) or EGFP alone (*lane 4*). The cell lysates were analyzed by Western blotting using anti-GFP (*A*) or anti-DOC2B antibodies (*B*). We compared fusion proteins with wild type DOC2B (*lane 1*) with the mutated variants M13 (*lane 2*) and TCT (*lane 3*). Please refer to Table I for detailed information about these mutations. *Right panel*, the EGFP tag does not influence the subcellular localization of DOC2B. A HEK293 cell expressing DOC2B-EGFP was visualized by anti-DOC2B immunostaining (*C*, *red*) or EGFP fluorescence (*D*, *green*). An overlay of both images is shown in *E*. A similar distribution was also observed by immunostaining cells that expressed untagged DOC2B (*F*, *red*). *Bar*, 10 μm.

as stable proteins with the expected molecular mass (Fig. 1). The full-length band was also recognized by a polyclonal antibody against DOC2B, whereas this antibody did not recognize EGFP alone (Fig. 1*B*). To investigate whether the EGFP tag could cause mislocalization of the expressed protein, we compared the cellular distribution of DOC2B-EGFP with that of untagged DOC2B. As shown in Fig. 1, *C* and *F*, both proteins produced a similar staining pattern using anti-DOC2B antibody. The immunostaining pattern was also similar to the fluorescence derived directly from the EGFP tag, except that the nuclear staining was relatively weak (Fig. 1, *C–E*). The antigenic region could be less accessible in nuclear-resident DOC2B-EGFP. As an additional control we replaced EGFP with a Myc tag, resulting in the same distribution under all conditions tested (data not shown). The distribution of DOC2B-Myc was again similar to that of the untagged DOC2B variants. From these control experiments, we conclude that the EGFP tag does not cause instability or artifacts in the subcellular localization of DOC2B.

Ca²⁺-dependent Localization of DOC2B-EGFP in Heterologous Cells—Under standard culture conditions, DOC2B-EGFP and DOC2B were homogenously distributed in the cytoplasm and nucleus of transfected HEK293 cells. The fluorescence intensity in the nucleus varied between cells. The same homogenous distribution was observed when the cells were incubated in basal buffer lacking Ca²⁺. In contrast, when the cells were incubated under conditions that elevate intracellular Ca²⁺ levels, DOC2B-EGFP showed a clearly distinct distribution characterized by an intense membrane-associated fluorescence and
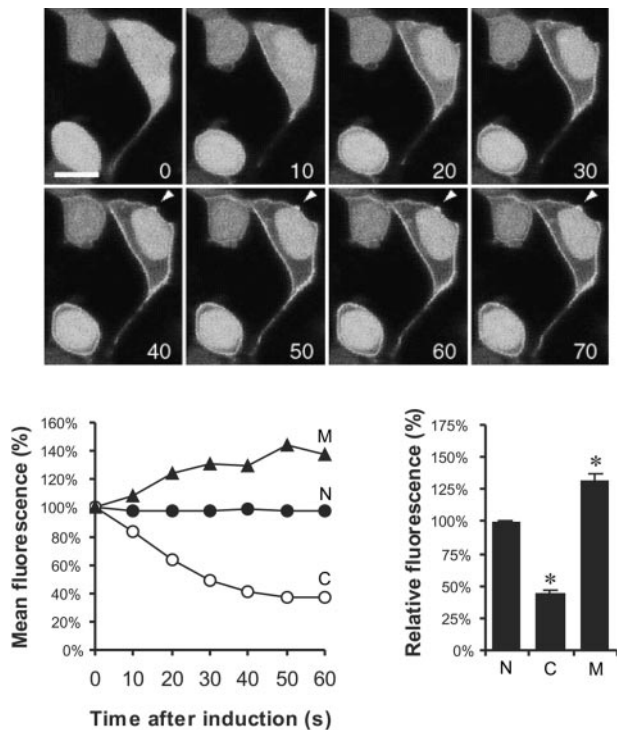
FIG. 2. **Subcellular localization of DOC2B-EGFP in response to Ca²⁺ influx.** *Upper panel*, live confocal imaging of HEK293 cells expressing DOC2B-EGFP. Transfected cells were incubated under basal conditions ($t = 0$). Ca²⁺ influx was induced by the addition of 1 μM A23187 and 3 mM CaCl₂ to the extracellular medium. The time after induction is indicated in seconds. *Bar*, 10 μm. *Lower left panel*, time-dependent change in fluorescence intensity in each cellular compartment after induction of Ca²⁺ influx. Values are expressed as percentages of the original fluorescence. *Lower right panel*, relative fluorescence in the nucleus (*N*), cytoplasm (*C*), and plasma membrane (*M*), presented as mean values of measurements in nine different cells. The *bars* indicate S.E.; *asterisks* indicate a significant change in fluorescence intensity ($p < 0.005$).

a loss of cytoplasmic fluorescence. This is shown in Fig. 2, where Ca²⁺ influx was induced by the extracellular application of 3 mM Ca²⁺ and a 1 μM concentration of the Ca²⁺ ionophore A23187. Following this treatment, a redistribution of the fusion protein was evident within less than 10 s. After stimulation, the membrane-associated fluorescence was not completely uniform along the cell membrane but showed focal accumulations (Fig. 2, *arrowheads*). The overall fluorescence intensity in the cytoplasm, membrane, and nucleus was quantitated at different time points in nine different cells. Cytoplasmic fluorescence decreased significantly ($p < 0.005$) to $44 \pm 3\%$ of the original value (mean $\pm$ S.E., $n = 9$), whereas the membrane-associated fluorescence increased significantly ($p < 0.005$) to $131 \pm 6\%$. The nuclear fluorescence intensity remained constant (mean value $101 \pm 1\%$). We therefore conclude that DOC2B-EGFP migrates from the cytoplasm to the plasma membrane after Ca²⁺ influx.

To exclude a nonspecific activity of the ionophore A23187 or its solvent, the ionophore was administered in the absence of extracellular Ca²⁺. This treatment did not induce any change in fluorescence distribution (Fig. 3, *C* and *G*). When 3 mM extracellular Ca²⁺ was applied without the ionophore, there was a small but detectable increase in plasma membrane-associated fluorescence (Fig. 3, *B* and *F*). This subtle change may reflect a small increase in intracellular Ca²⁺ as a consequence of the extracellular rise in Ca²⁺ concentration. Only after application of both components at the same time did a quantitative translocation of the fluorescent protein occur (Fig. 3, *D* and *H*). We also investigated whether the translocation
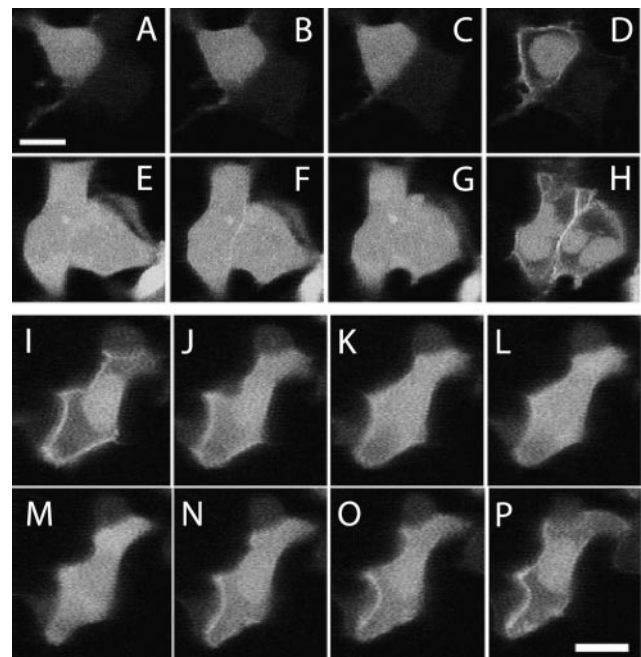

FIG. 3. *Upper panel*, both Ca²⁺ and ionophore A23187 are required for DOC2B-EGFP translocation. Live confocal imaging is shown of HEK293 cells, incubated 48 h post-transfection at 37 °C in basal medium without supplement (*A* and *E*) or supplemented with 3 mM CaCl₂ (*B* and *F*), 1 μM A23187 (*C* and *G*), or both (*D* and *H*). *Lower panel*, the translocation of DOC2B-EGFP is both reversible and repeatable. HEK293 cells expressing DOC2B-EGFP were stimulated by the administration of 3 mM Ca²⁺ and 1 μM A23187 (*I*). Subsequently, the medium was replaced with basal buffer containing 3 mM EGTA, which resulted in a reversal of the translocation (*J–M*). The medium was then replaced with buffer containing 3 mM Ca²⁺ and 1 μM A23187 (*N–P*). *Bars*, 10 μm.

was reversible and repeatable (Fig. 3, *I–P*). Cells expressing DOC2B-EGFP were stimulated as described above. The medium was then replaced to wash out the ionophore, resulting in a reversal of the membrane-associated fluorescence to a homogenous cytoplasmic distribution. An additional replacement with stimulation medium again induced a translocation of DOC2B-EGFP to the plasma membrane. These control experiments indicate that the observed translocation of DOC2B-EGFP requires Ca²⁺ influx and is not caused by irreversible cell damage due to the stimulation treatment.

The Ca²⁺-induced Translocation of DOC2B Is Independent of Munc13 and Tctex-1 Binding—The binding of DOC2B to the plasma membrane could be mediated by accessory proteins or by direct binding of one of the C2 domains to the phospholipid bilayer. To investigate the participation of each functional domain, we introduced targeted mutations in the N-terminal domain to block the interaction with Munc13 and Tctex-1 (a subunit of the cytoplasmic dynein complex), respectively (Fig. 4) (see Table I). All mutants expressed showed the expected molecular mass without visible signs of degradation in Western blotting (Fig. 1).

Although HEK293 cells do not express Munc13 to detectable amounts as analyzed by immunoblotting, the above experiments do not exclude the involvement of extremely low amounts of Munc13. Therefore, we introduced a previously characterized mutation in the Munc13-interacting domain of DOC2B that abolishes Munc13 binding (12) (see Table I). To confirm that this mutation blocks the Munc13-dependent translocation triggered by phorbolesters, we first co-expressed DOC2B-EGFP and Munc13-1 in HEK293 cells. In agreement with previously reported studies (11), the administration of the phorbolester phorbol 12-myristate 13-acetate resulted in a translocation of DOC2B-EGFP (Fig. 5A). When the same treat-

FIG. 4. **Ca²⁺-dependent localization of mutant DOC2B-EGFP variants.** HEK293 cells were transfected with full-length DOC2B with EGFP attached to its carboxyl terminus. Besides wild type DOC2B (*WT*), we also analyzed the mutants named TCT and M13 (see Table I) and, as controls, EGFP alone (*GFP*), PKC-α, and PKC-γ. Prior to fixation, the cells were incubated for 10 min under basal conditions (indicated by a *minus sign*) or in the presence of 1 μM A23187 and 3 mM Ca²⁺ (indicated by a *plus sign*). Alternatively, the cells were stimulated by 10 mM Ba²⁺ added to the basal medium (*inset*). *Bars*, 10 μm.
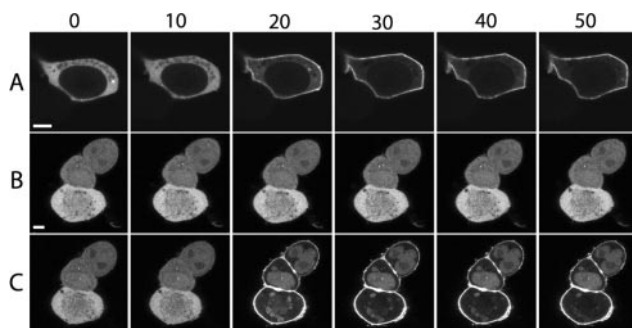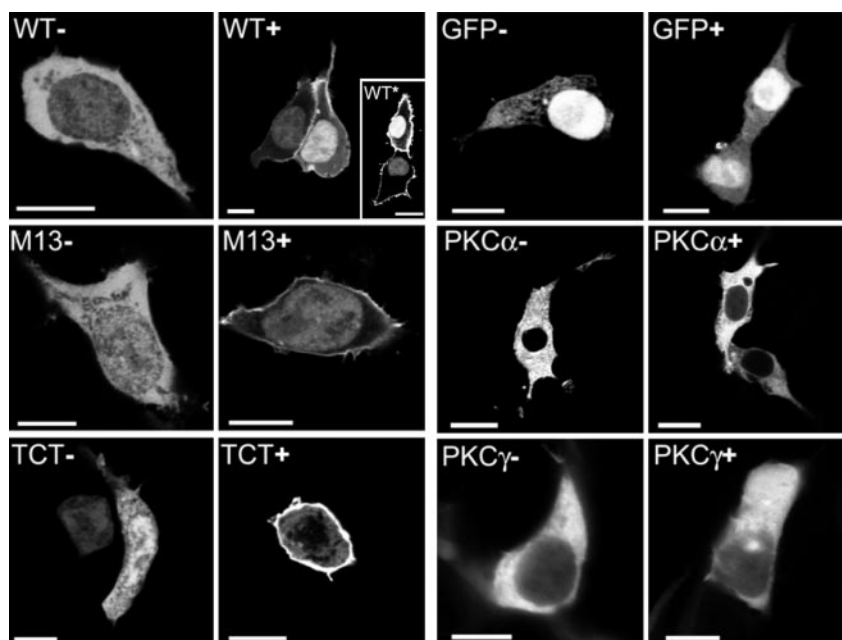

FIG. 5. **Mutagenesis at the Munc13-interacting domain blocks phorbolester-induced membrane binding by DOC2B-EGFP.** HEK293 cells co-expressing Munc13.1 and DOC2B-EGFP were stimulated by application of the phorbolester phorbol 12-myristate 13-acetate to a final concentration of 100 nM, resulting in a translocation of the fluorescent DOC2B-EGFP protein to the membrane (*A*) (the time after induction is indicated in seconds). When wild type DOC2B was replaced with its mutated variant M13 (see Table I), the same treatment did not induce translocation (*B*). Stimulation of the same cell with 3 mM Ca²⁺ and 1 μM A23187, in contrast, readily induced a translocation of the mutated DOC2B-EGFP protein (*C*). *Bars*, 5 μm.

FIG. 6. *Upper panel*, live confocal imaging of the DOC2B-EGFP mutant designated M13. The time after the addition of 3 mM Ca²⁺ and 1 μM A23187 is indicated in seconds. The mutation is described in Table I. *Bar*, 10 μm. *Lower left panel*, time-dependent change in fluorescence intensity in each cellular compartment. Values are expressed as percentages of the original fluorescence. *Lower right panel*, relative fluorescence in the nucleus (*N*), cytoplasm (*C*), and cell membrane (*M*) after the addition of 1 μM A23187 and 3 mM CaCl₂, presented as mean values of five measurements in five different cells. The *bars* indicate S.E.; the *asterisk* indicates a significant change in fluorescence intensity ($p < 0.005$).

ment was performed with the mutated DOC2B-EGFP variant (M13), no translocation was observed (Fig. 5*B*). However, when the same cells were stimulated with 3 mM Ca²⁺ and 1 μM ionophore, the mutated protein readily translocated to the plasma membrane (Fig. 5*C*). Having confirmed that the M13 mutation effectively blocks the phorbolester-induced translocation of DOC2B-EGFP, we next expressed mutated DOC2B-EGFP without co-expression of Munc13 (Fig. 6). Upon induction of Ca²⁺ influx, the mutant fusion protein rapidly associated with the plasma membrane in a way that was indistinguishable from wild type DOC2B-EGFP. From these data, we conclude that Ca²⁺-induced translocation of DOC2B is not mediated by binding to Munc13.

Another mutation named TCT (20) (see Table I) was introduced in the N-terminal domain to assess the role of Tctex-1 binding in the Ca²⁺-induced translocation of DOC2B-EGFP. Again, this mutation did not influence the basal localization or translocation activity of the fusion protein (Fig. 4, *TCT⁻* and *TCT⁺*), indicating that the interaction with the dynein-binding motif at the N terminus of DOC2B is not involved.

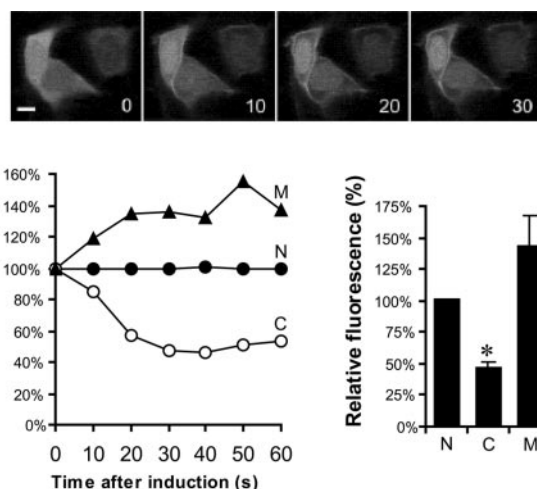Since the Ca²⁺-induced recruitment of DOC2B-EGFP to the plasma membrane binding is independent of Munc13 and Tctex-1, the most likely explanation for this phenomenon is a Ca²⁺-triggered C2 domain activation. To test this hypothesis, we expressed and purified our full-length DOC2B construct in the form of a bacterial fusion protein with GST and analyzed whether it could bind phospholipids in a Ca²⁺-dependent manner. The GST-DOC2B fusion protein (calculated molecular mass, 72 kDa) appeared in SDS-PAGE as a predominant band at the expected height (Fig. 7*A*). Several additional bands were visible that corresponded with a lower molecular mass, indicative of a limited amount of protein degradation (*asterisk*). The GST-DOC2B protein alone was sufficient to bind liposomes in a Ca²⁺-dependent manner, showing a half-maximal binding activity of ~5 μM free Ca²⁺. This Ca²⁺-dependent phospholipid binding activity is comparable with that of an isolated C2A
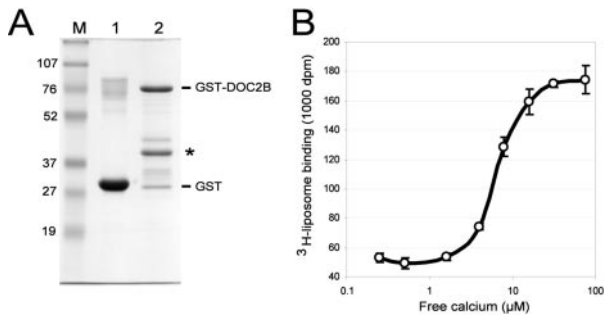
FIG. 7. **Ca²⁺-dependent phospholipid binding by purified GST-DOC2B.** *A*, purification of a bacterial fusion protein composed of GST and full-length DOC2B. GST (*lane 1*) and GST-DOC2B (*lane 2*) were analyzed by SDS-PAGE and Coomassie Brilliant Blue staining. *M*, marker lane. In addition to the full-length protein, several weak additional bands indicate a limited amount of protein degradation (*asterisk*). *Panel B*, binding of ^{3}H-labeled liposomes to immobilized GST-DOC2B as a function of the free Ca^{2+} concentration. Liposomes were prepared from phosphatidylcholine and phosphatidylserine in a 5:2 (w/w) ratio. The *error bars* indicate S.E. ($n = 3$).

domain fragment as shown previously (8). These results indicate that the Ca^{2+}-dependent plasma membrane association of DOC2B is primarily mediated by the C2 domains.

Kinetic Properties of Ca²⁺-induced Plasma Membrane Binding in PC12 Cells—The above results showed that DOC2B-EGFP is recruited by Ca^{2+} to the plasma membrane in heterologous cells. We also used PC12 cells, derived from chromaffin cells of the adrenal gland, to test whether a similar translocation occurred in cells that are specialized in Ca^{2+}-dependent exocytosis. Transfected PC12 cells showed the same homogenous distribution of DOC2B-EGFP under basal conditions and the same translocation of the protein to the plasma membrane after stimulation of Ca^{2+} influx (analyzed by live confocal imaging; data not shown).

For an accurate kinetic analysis of the Ca^{2+}-induced plasma membrane binding, we used the TIRF microscopy technique. This technique specifically records fluorescence at the plasma membrane with a high temporal resolution. A typical experiment is depicted in Fig. 8. PC12 cells expressing DOC2B-EGFP were analyzed during 30 s for their fluorescence intensity at the membrane. After an initial incubation in basal solution, the cells were depolarized for 10 s to induce Ca^{2+} influx, followed by a second incubation in basal solution. The membrane depolarization induced a marked increase in DOC2B-EGFP fluorescence, followed after removal of the stimulus by a complete reversal to the original fluorescence intensity (Fig. 8). On average, among nine individual cells, the membrane-associated fluorescence increased 3-fold. The rise and decay components of the observed changes in membrane-associated fluorescence followed different kinetic rates, which were optimally fitted by monoexponential curves with half-time constants of 2.05 ± 0.11 and 7.9 ± 0.6 s, respectively (mean $\pm$ S.E., $n = 9$). In conclusion, the Ca^{2+}-induced membrane association of DOC2B-EGFP is rapid and also occurs in PC12 cells that are specialized in Ca^{2+}-triggered exocytosis.

Localization of DOC2B in Neurons—Since DOC2B is highly expressed in neurons of the brain, we next asked whether the Ca^{2+}-induced plasma membrane association also occurs in neurons. Cultured mouse neurons were transduced with lentiviral expression vectors (21) encoding DOC2B-EGFP. The level of DOC2B-EGFP expression could be detected 7 days after transduction and was sustained to the maximum period analyzed (*i.e.* 8 weeks post-transduction), indicating that virus-encoded DOC2B-EGFP expression does not compromise the viability of neurons. The recombinant protein was found throughout the neuron, including the soma and the neurite
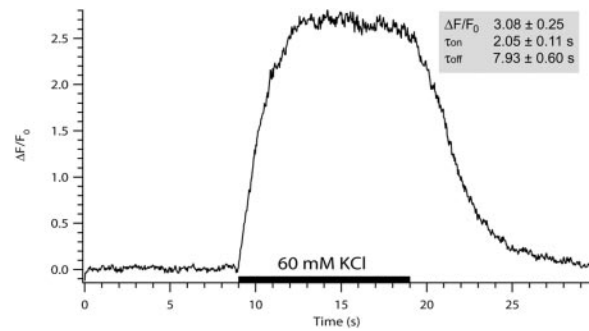

FIG. 8. **Kinetics of Ca²⁺-induced membrane association.** Plasma membrane-associated DOC2B-EGFP was analyzed in PC12 cells by TIRF microscopy. The *trace* shows an example recording of fluorescence intensity during 30 s. The *bar* indicates potassium-induced depolarization of the cell for 10 s. The *inset* shows averaged parameters measured from nine individual transfected cells. $\Delta F/F_0$ represents the change in fluorescence intensity relative to the original value. τ_{on} and τ_{off} represent the half-time constants (in seconds) of fitted monoexponential curves for membrane binding and release, respectively.

extensions (Fig. 9*A*; a three-dimensional rendering of this image is available as Supplemental Data). The fusion protein was also present in local accumulations along the dendritic and axonal extensions. Neuronal identity was confirmed by counterstaining for the neuronal dendritic marker, MAP2 (Fig. 9, *B–H*). Under normal culture conditions (*i.e.* at physiological concentrations of intracellular Ca^{2+}), we observed a significant cell-to-cell variation in the localization of DOC2B-EGFP. Typically, the fluorescence was found partly at the membrane and in the cytoplasmic compartment (Fig. 9*B*). Interestingly, DOC2B-EGFP also associated with intracellular membranes in neurons. To investigate whether the partial membrane association of DOC2B was due to the endogenous levels of intracellular Ca^{2+}, we incubated the neurons in basal buffer lacking Ca^{2+}. This treatment indeed resulted in a cytoplasmic distribution of the fluorescent signal (Fig. 9*C*). Stimulation of neurons by application of a depolarizing solution readily induced plasma membrane association of DOC2B-EGFP within 10 s (Fig. 9*D*) as expected. A similar translocation was induced by treatment of the neurons with a Ca^{2+} ionophore (data not shown). The translocation of DOC2B-EGFP was reversible and repeatable, as confirmed by live confocal imaging (Fig. 10). Thus, our results indicate that the Ca^{2+}-induced plasma membrane binding activity of DOC2B-EGFP is relevant in neurons and that endogenous Ca^{2+} concentrations in cultured neurons are in the appropriate range to dynamically influence the membrane binding activity of DOC2B.

We also tested the expression pattern in neurons of the mutant DOC2B-EGFP variants designated M13 and TCT. The results corresponded with those obtained in HEK293 cells. The M13 mutant showed a cytoplasmic fluorescence pattern in basal buffer lacking Ca^{2+} (Fig. 9*E*). After the stimulation of Ca^{2+} influx, the fluorescence shifted to a membrane-associated pattern (Fig. 9*F*). Under standard culture conditions, fluorescence was observed both in the cytoplasmic compartment and at the membrane (not shown). The same dynamic behavior was observed for the mutant TCT (Fig. 8, *G* and *H*). Therefore, also in neurons, the interactions of DOC2B with Munc13 and Tctex-1 are not required for its Ca^{2+}-induced recruitment.

DISCUSSION

In this study, we investigated the intracellular localization of DOC2B, a high affinity Ca^{2+} sensor with a putative function in regulated exocytosis. We found that Ca^{2+} influx is sufficient to induce a rapid and complete translocation of cytosolic DOC2B-EGFP to the target membrane in living cells. This activity was observed in heterologous cells and PC12 cells (specialized in
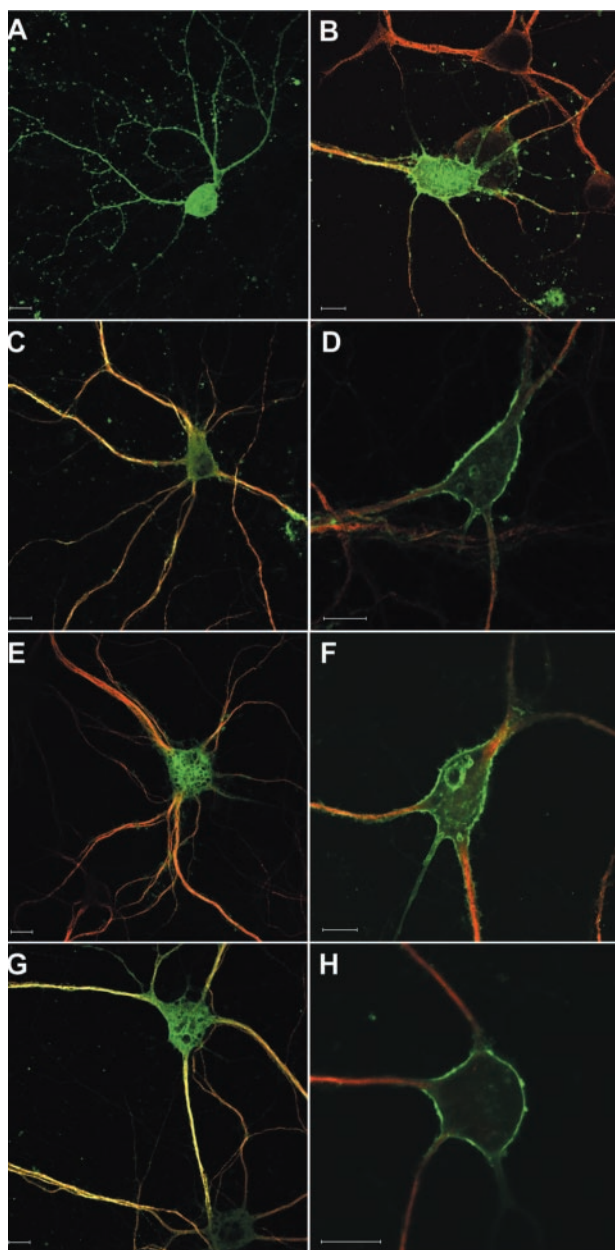
FIG. 9. **Expression of DOC2B-EGFP fusion protein in cultured mouse hippocampal neurons.** *A*, vertical projection of multiple confocal planes showing that DOC2B-EGFP was expressed in the neuronal soma and throughout the neurite extensions. *B–H*, confocal images of neurons expressing DOC2B-EGFP (*green*) counterstained for the neuronal dendritic marker MAP2 (*red*) to confirm the neuronal identity. Besides the wild type form of DOC2B (*B–D*), the neurons expressed fusion proteins containing mutated variants designated M13 (*E* and *F*) and TCT (*G* and *H*). The neurons were incubated in basal buffer lacking Ca^{2+} (*A*, *C*, *E*, and *G*), normal culture medium (*B*), or depolarizing buffer containing 60 mM KCl (*D*, *F*, and *H*). *Bars*, 10 μM. A Quicktime movie showing a three-dimensional rendering of the neuron shown in *A* is available as Supplemental Data.

Ca^{2+}-dependent large dense core vesicle exocytosis). Moreover, the Ca^{2+}-induced translocation also occurred in neurons, known to express endogenous DOC2B at high levels (7).

The presence of an EGFP tag at the C terminus of full-length DOC2B did not influence its cellular localization. As shown by Western blotting, the recombinant fusion proteins were soluble and stable. Furthermore, the distribution of the fusion protein was similar to untagged DOC2B. Polyclonal antibodies produced a similar staining pattern compared with the direct fluorescence from DOC2B-EGFP, but the immunostaining was
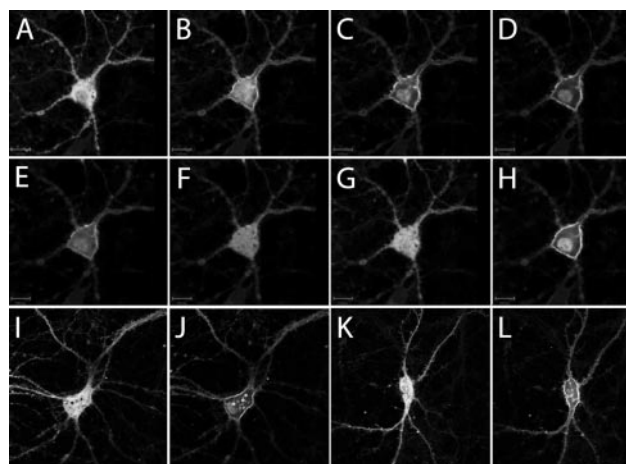

FIG. 10. **Live confocal imaging analysis of three neurons expressing DOC2B-EGFP.** *A–H*, a neuron expressing DOC2B-EGFP was incubated subsequently in basal buffer containing 3 mM EGTA (*A*), in depolarizing buffer containing 60 mM KCl (*B–D*), in basal buffer again (*E–G*), and in depolarizing buffer again (*H*). The incubation times were 1, 5, and 30 s in depolarizing buffer (*B–D*); 5, 10, and 30 s in EGTA-containing buffer (*E–G*); and 1 s in depolarizing buffer (*H*), respectively. *Bars*, 50 μM. *Panels I* and *J* and *panels K* and *L* show a similar potassium-induced translocation in two other neurons. Quicktime movies corresponding to *panels I* and *J* and *panels K* and *L* are available as Supplemental Data.

relatively weak in the nuclear compartment. We speculate that DOC2B-EGFP in the nucleus represents an incorrectly folded subpopulation of the overexpressed recombinant protein that is not recognized by the antibody. DOC2B contains several basic amino acid clusters that are normally buried in the C2 domain structure and could aberrantly act as a nuclear localization signal in misfolded protein. Therefore, the observed cell-to-cell variation in nuclear fluorescence may correspond with variations in the cellular expression level and hence with the accuracy of protein folding.

The Ca^{2+}-induced mobilization of DOC2B represents a novel mechanism, distinct from the previously described Munc13-dependent translocation in response to diacylglycerol synthesis (11). This conclusion is based on the following considerations. First, DOC2B-EGFP translocated in HEK293 cells that do not express Munc13. Second, mutation of the Munc13-interacting domain of DOC2B did not inhibit Ca^{2+}-induced membrane binding, but it completely blocked the phorbolester-induced translocation. This mutation was previously demonstrated to block Munc13-binding activity of this domain in a cell-free system (12). In this study, we provide a further characterization of the same mutation and conclude that it does not disrupt DOC2B stability, basal localization, and Ca^{2+}-induced membrane binding. The selective inhibition of diacylglycerol-induced Munc13 binding in this mutant, however, makes this mutant protein a valuable tool to dissect the phorbolester- and Ca^{2+}-dependent activation pathways in future research. Taken together, our data fully support the previously identified translocation in response to phorbolester stimulation, a phenomenon that requires the presence of Munc13. In addition, we have demonstrated that Ca^{2+} elevations alone also recruit DOC2B to the plasma membrane, and both mechanisms are truly independent. In Munc13-expressing cells, both mechanisms probably converge to achieve a synergistic activation of DOC2B by Ca^{2+} influx and diacylglycerol synthesis near active exocytotic sites.

The Ca^{2+}-induced recruitment most likely involves a direct interaction of its C2 domains with the phospholipid layer of the target membrane. In a cell-free assay, purified DOC2B (expressed as a bacterial fusion protein with GST) bound to syn-

thetic liposomes containing phosphatidylcholine and phosphatidylserine in a Ca^{2+}-dependent way. Our results are in accordance with a previous study that showed liposome binding by a DOC2B fragment containing only the C2A domain, showing a similar dependence on the free Ca^{2+} concentration (8). By contrast, the isolated C2B domain did not show Ca^{2+}-induced phopholipid affinity *in vitro* (8). Therefore, the most simple explanation for the Ca^{2+}-induced translocation of DOC2B is that Ca^{2+} causes a conformational or electrostatic change through binding to the C2A domain, resulting in an increased affinity of DOC2B for phospholipids of the plasma membrane. Similar Ca^{2+}-dependent phospholipid-C2 domain interactions were observed previously in several other proteins (*e.g.* synaptotagmins and PKC isoforms) (see Ref. 22). As prototype C2 proteins with a Ca^{2+}-dependent plasma membrane binding activity (18, 19), we also tested the localization of PKCα and -γ in our assay. Remarkably, under the conditions used (1 μM ionophore), the DOC2B-EGFP translocation was clearly more pronounced than that of the PKC isoforms, which require more stringent concentrations for their activation (*e.g.* 10–80 μM ionophore), suggesting that DOC2B is activated by relatively low concentrations of intracellular Ca^{2+}.

Several lines of evidence have indicated a regulatory role of DOC2 proteins in Ca^{2+}-induced exocytosis, located upstream from the actual fusion event (9, 12, 13, 23–25). This is also suggested by the interaction of DOC2 with Munc18 and Munc13, both essential components of the vesicle docking/priming machinery (3, 14). Our results are fully consistent with a putative function in activity-dependent enhancement of exocytosis, considering that 1) the speed of translocation is sufficiently high and 2) the translocation occurs at intracellular Ca^{2+} levels within the dynamic physiological range. With respect to the speed of translocation, we observed in our experiments in PC12 cells that DOC2B-EGFP bound to the membrane with a monoexponential half-time of 2.05 s. Of the distinct components involved in activity-dependent enhancement, this kinetic rate corresponds best with the relatively slow components defined as augmentation (~1 s) and potentiation (~10 s) (1). These components are thought to be activated by residual Ca^{2+} concentrations at locations distant from the Ca^{2+} channels. The translocation speed in response to Ca^{2+} is also comparable with the time scale of diacylglycerol-mediated potentiation, known to require Munc13 (26) and its interaction with DOC2 (12, 13). The diacylglycerol/Munc13-induced translocation of DOC2B to the plasma membrane, on the other hand, has been observed in the range of 5–30 min previously (11) and after 30–50 s in our experiments. Thus, the kinetic parameters from our studies are consistent with a proposed function in activity-dependent enhancement of exocytosis.

A putative role in activity-dependent enhancement of exocytosis is furthermore supported by the apparent Ca^{2+} sensitivity of DOC2B. Estimated concentrations of intracellular Ca^{2+} in neurons range from 10–100 μM during Ca^{2+} channel opening to ~1 μM during delayed phases after Ca^{2+} influx and ~100 nm under resting conditions (2, 27). The peak levels are only reached transiently (for milliseconds) in close proximity to activated Ca^{2+} channels. For DOC2B, half-maximal phospholipid binding by the isolated C2A domain occurs at a concentration of 1 μM (8). We show here that in cultured neurons expressing full-length DOC2B, a partial membrane association occurs already at physiological Ca^{2+} concentrations. Depletion of Ca^{2+} from the medium reversed this membrane association. Hence,

the observed variability between individual cells was probably caused by differences in intracellular Ca^{2+} levels. This implicates that DOC2B translocation occurs in living cells that have accumulated relatively high intracellular Ca^{2+} concentrations as a result of their physiological activity, further supporting a function in activity-dependent enhancement of exocytosis.

Combining the available data, we propose that DOC2B couples intracellular Ca^{2+} elevations to the activity-dependent enhancement of exocytosis by the following mechanism. During the temporary rise in intracellular Ca^{2+} after exocytotic activity, DOC2B rapidly associates with the target membrane. Independently, DOC2B may engage into a membrane-bound complex with Munc13 in response to local diacylglycerol production (10, 11). Through one or more downstream interactions that remain to be elucidated, this DOC2B-Munc13 interaction finally results in the activity-dependent enhancement of exocytotic strength.

REFERENCES

1. Fisher, S. A., Fischer, T. M., and Carew, T. J. (1997) *Trends Neurosci.* **20,** 170–177
2. Zucker, R. S., and Regehr, W. G. (2002) *Annu. Rev. Physiol.* **64,** 355–405
3. Augustin, I., Rosenmund, C., Sudhof, T. C., and Brose, N. (1999) *Nature* **400,** 457–461
4. Rhee, J. S., Betz, A., Pyott, S., Reim, K., Varoqueaux, F., Augustin, I., Hesse, D., Sudhof, T. C., Takahashi, M., Rosenmund, C., and Brose, N. (2002) *Cell* **108,** 121–133
5. Fukuda, M., and Mikoshiba, K. (2000) *Biochem. Biophys. Res. Commun.* **276,** 626–632
6. Sakaguchi, G., Orita, S., Maeda, M., Igarashi, H., and Takai, Y. (1995) *Biochem. Biophys. Res. Commun.* **217,** 1053–1061
7. Verhage, M., de Vries, K. J., Roshol, H., Burbach, J. P., Gispen, W. H., and Sudhof, T. C. (1997) *Neuron* **18,** 453–461
8. Kojima, T., Fukuda, M., Aruga, J., and Mikoshiba, K. (1996) *J. Biochem. (Tokyo)* **120,** 671–676
9. Orita, S., Sasaki, T., Komuro, R., Sakaguchi, G., Maeda, M., Igarashi, H., and Takai, Y. (1996) *J. Biol. Chem.* **271,** 7257–7260
10. Orita, S., Naito, A., Sakaguchi, G., Maeda, M., Igarashi, H., Sasaki, T., and Takai, Y. (1997) *J. Biol. Chem.* **272,** 16081–16084
11. Duncan, R. R., Betz, A., Shipston, M. J., Brose, N., and Chow, R. H. (1999) *J. Biol. Chem.* **274,** 27347–27350
12. Mochida, S., Orita, S., Sakaguchi, G., Sasaki, T., and Takai, Y. (1998) *Proc. Natl. Acad. Sci. U. S. A.* **95,** 11418–11422
13. Hori, T., Takai, Y., and Takahashi, T. (1999) *J. Neurosci.* **19,** 7262–7267
14. Verhage, M., Maia, A. S., Plomp, J. J., Brussaard, A. B., Heeroma, J. H., Vermeer, H., Toonen, R. F., Hammer, R. E., van den Berg, T. K., Missler, M., Geuze, H. J., and Sudhof, T. C. (2000) *Science* **287,** 864–869
15. Voets, T., Toonen, R. F., Brian, E. C., de Wit, H., Moser, T., Rettig, J., Sudhof, T. C., Neher, E., and Verhage, M. (2001) *Neuron* **31,** 581–591
16. Toonen, R. F., and Verhage, M. (2003) *Trends Cell Biol.* **13,** 177–186
17. Brose, N., Hofmann, K., Hata, Y., and Sudhof, T. C. (1995) *J. Biol. Chem.* **270,** 25273–25280
18. Vallentin, A., Prevostel, C., Fauquier, T., Bonnefont, X., and Joubert, D. (2000) *J. Biol. Chem.* **275,** 6014–6021
19. Sakai, N., Sasaki, K., Ikegaki, N., Shirai, Y., Ono, Y., and Saito, N. (1997) *J. Cell Biol.* **139,** 1465–1476
20. Nagano, F., Orita, S., Sasaki, T., Naito, A., Sakaguchi, G., Maeda, M., Watanabe, T., Kominami, E., Uchiyama, Y., and Takai, Y. (1998) *J. Biol. Chem.* **273,** 30065–30068
21. Naldini, L., Blomer, U., Gallay, P., Ory, D., Mulligan, R., Gage, F. H., Verma, I. M., and Trono, D. (1996) *Science* **272,** 263–267
22. Rizo, J., and Sudhof, T. C. (1998) *J. Biol. Chem.* **273,** 15879–15882
23. Duncan, R. R., Shipston, M. J., and Chow, R. H. (2000) *Biochimie (Paris)* **82,** 421–426
24. Orita, S., Sasaki, T., and Takai, Y. (2001) *Methods Enzymol.* **329,** 83–90
25. Sakaguchi, G., Manabe, T., Kobayashi, K., Orita, S., Sasaki, T., Naito, A., Maeda, M., Igarashi, H., Katsuura, G., Nishioka, H., Mizoguchi, A., Itohara, S., Takahashi, T., and Takai, Y. (1999) *Eur. J. Neurosci.* **11,** 4262–4268
26. Brose, N., and Rosenmund, C. (2002) *J. Cell Sci.* **115,** 4399–4411
27. Bollmann, J. H., Sakmann, B., and Borst, J. G. (2000) *Science* **289,** 953–957